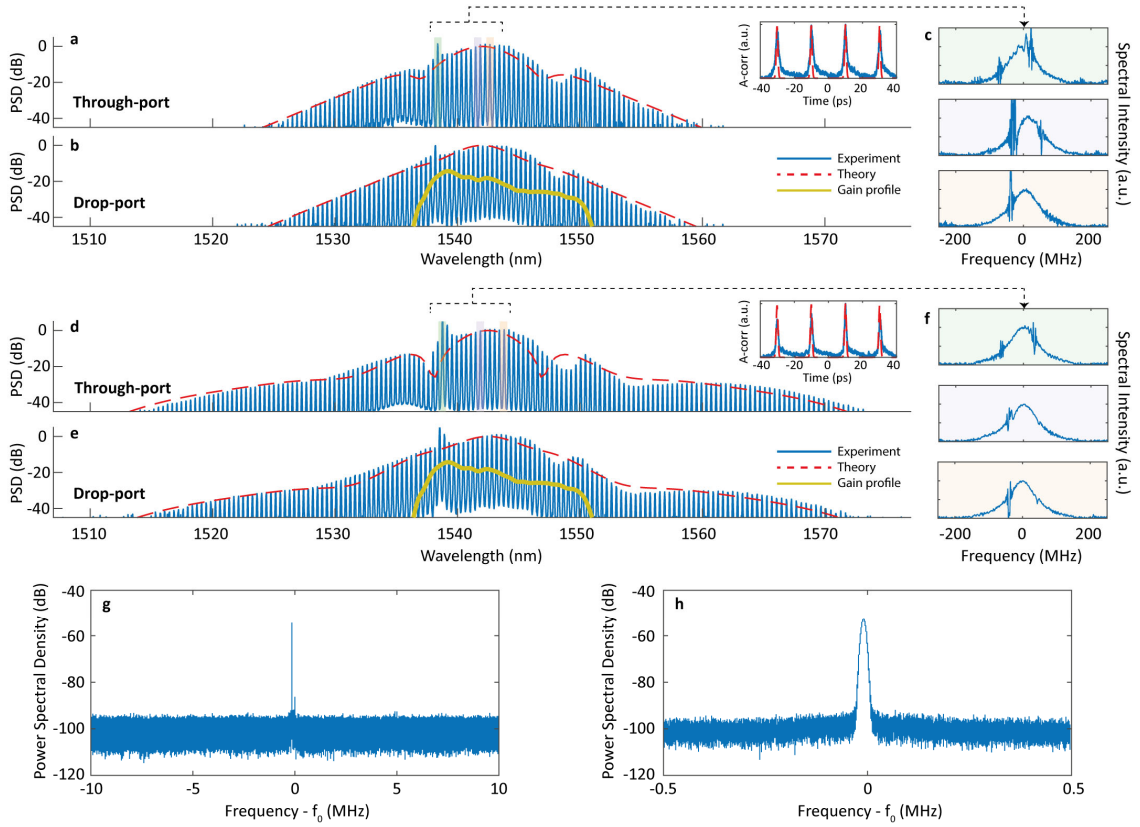

Figure E1 Characterisation of the soliton state a-c Example soliton state, obtained with a 350 mW pump at 980 nm. Experimentally obtained optical spectra of a single soliton (blue) with their theoretical fit (red dashed) at the **a** 'through' and **b** 'drop' ports. In the fit, we use g=0.08 and Δ=0.46, with the other parameter reported in the Methods. The operational EDFA gain bandwidth is indicated by the overlay in yellow. The input power to the microchip is 44 mW and the measured output powers are 4 mW at the 'through', and 6.5 mW in the intracavity 'drop' ports, respectively. The insets correspond to the autocorrelation trace, clearly showing one peak per microcavity round-trip. **c** Three examples of the intracavity spectrum (blue), displaying the lasing modes within each microcavity resonance and corresponding to the highlighted wavelengths. While the modes are all red detuned, we observe in the mode around 1538 nm, where the peak of the Erbium is located, the coexistence of the soliton red detuned mode with a blue-detuned continuous wave mode in **b**. **d-f** Same as **a-c**, for a single soliton with a slightly higher pump power of 360 mW at 980 nm. In the fit we use g=0.1 and Δ=0.4, with the other parameter reported in the methods. The input power to the microchip is 63 mW and the measured output powers are 5 mW at the 'through', and 8.3 mW at the intracavity 'drop' ports. The spectral shape is theoretically fitted by the same model. **e** Same as **c**, for the spectrum shown in **d**. **g** Radio-frequency spectrum measured around the repetition rate frequency via heterodyne modulation. A small portion of the 'through' output signal is processed with an electro-optic modulator, leading to additional sidebands around each of the original comb lines. We considered the third harmonic sidebands, and then set the modulation frequency such that the interaction between adjacent comb-lines produced a f_0=500 MHz beat-note. Electrical spectrum analyser trace of the signal derived from the amplified photodiode after the electroptic modulation, at 50 MHz span, and resolution bandwidth of 30 kHz. **h** Same as (g) but with 1 MHz span, and resolution bandwidth of 10 kHz.

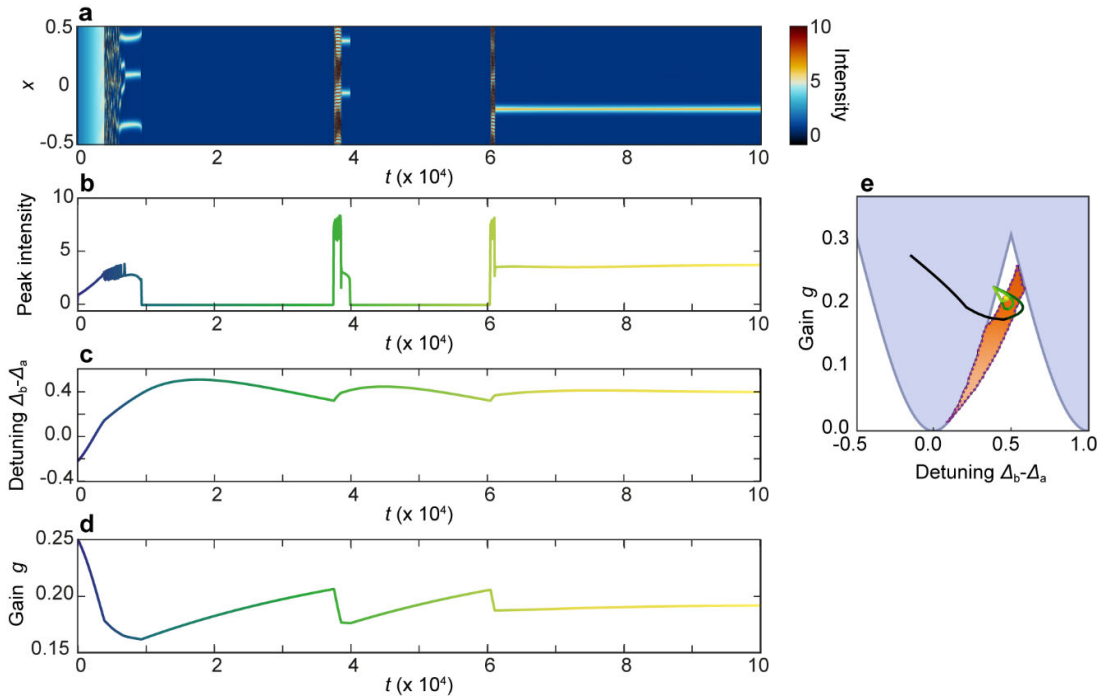

Figure E2 Start-up in the presence of gain-induced nonlinearity and thermal nonlinearity: single soliton formation. Numerical propagation for Eqs. (1-4) in Supplementary Section S1, modelling a microresonator-filtered fibre laser with the inclusion of a saturable gain and gain-induced nonlinearity in the amplifying cavity, and a thermal nonlinearity in the microcavity. The system parameters are $\Gamma_T = 5, \tau_T = 8 \times 10^3, \eta = 0.4, \tau_g = 4 \times 10^4, \Theta = -13, g = 0.25$, and $\Delta + \Theta g_P = -0.21$. **a** Pseudo-colour map of the electric field intensity in the microcavity, in the normalised units of Eqs. (1-4), as a function of the position in the microresonator x (which is normalised against the microcavity roundtrips) and time t (which is normalised against the main-cavity roundtrips). **b** Temporal evolution of the peak intensity. The colours varying for increasing times matches with the plot inside panel e (showing the attractor). **c** Temporal evolution of the effective detuning $\Delta_b - \Delta_a$. The colours varying for increasing times matches with the plot in panel e. **d** Temporal evolution of the gain. The colours varying for increasing times matches with the plot in panel e. **e** Map of the attractor for the peak intensity, detuning and gain, as in panel c-d, following the colour code of panel b as a function of time. The attractor is superimposed to the soliton (orange) and zero state (blue) stability regions, as in Fig. 2a of the main text.

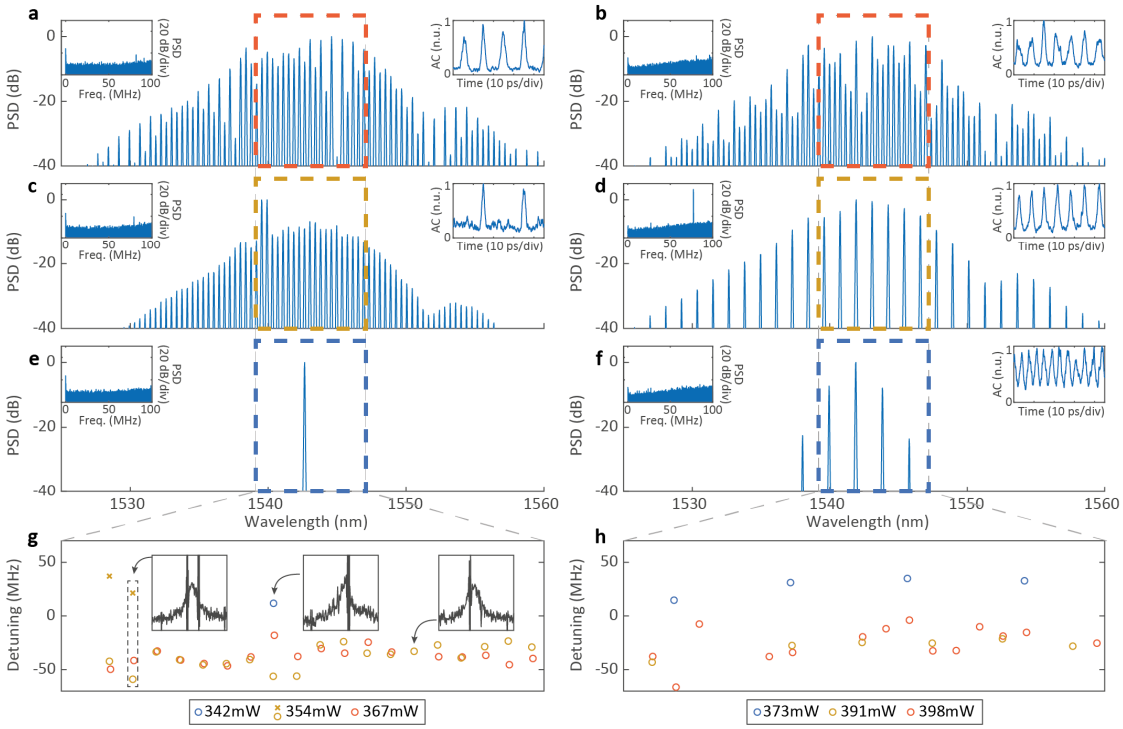

Figure E3 Summary of laser scanning-spectroscopy measurements. **a** Power spectral density (PSD) of optical and radio-frequency spectra (left inset) with autocorrelation (right inset) for an EDFA pump power of 367 mW, for the system with 16 dB losses. **b** Same as panel a, for an EDFA pump power of 398 mW, for the system with 14 dB losses. **c** Same as panel a, for an EDFA pump power of 354 mW. **d** Same as panel b for an EDFA pump power of 391 mW. **e** Same as panel a, for an EDFA power of 342 mW. **f** Same as panel b for an EDFA power of 373 mW. **g** The insets show three typical laser scanning spectroscopy measurements for a red-detuned oscillating line (right), blue-detuned line (centre), and coexistence of two oscillating modes (left). From these measurements, it is possible to extract the absolute frequency position of the oscillating line and the centre of the microcavity resonance. We define their difference as the frequency detuning of the lasing states in operating conditions. The distribution of the individual mode detunings across the wavelength span highlighted by the grey dashed lines for 16 dB intracavity losses and EDFA pump powers of 342 mW, 354 mW and 367 mW are shown in blue, yellow, and red, respectively. **h** Same as panel g, for the system at 14 dB intracavity losses, and for EDFA pump powers of 373 mW, 391 mW and 398 mW.

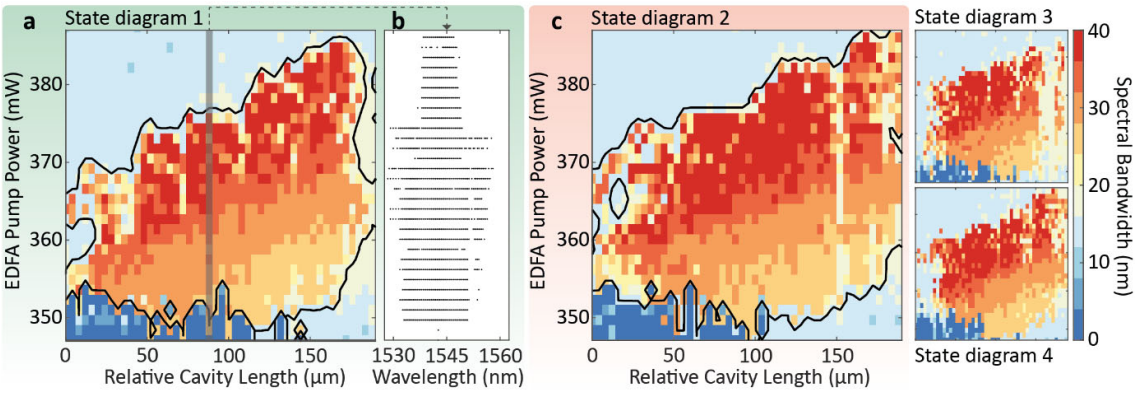

Figure E4. Repetitions of experimental state diagrams for the microresonator-filtered fibre laser with intracavity losses set to 16 dB. a Optical spectral bandwidth (calculated as the bandwidth at -40dB from the maximum) of the laser states, as a function of the cavity length and EDFA pump power. The soliton states are found in the yellow to red region with the broadest bandwidths, while CW states are in blue. Outside these regions, roughly defined by the black lines, the lasing regime is unstable. During the 10-hour experiment performed to acquire the data, the temperature was maintained at 40° C to within a fluctuation of a few degrees. **b** Optical spectra of the states along with the 92 μm delay position, identified by the grey line in panel a. The black dots represent the frequency position relative to the maximum value of each comb mode. **c** Repetition of the same experimental map, with two further repetitions on the insets, acquired immediately after the map in panel a, over subsequent 10-hour long experiments.

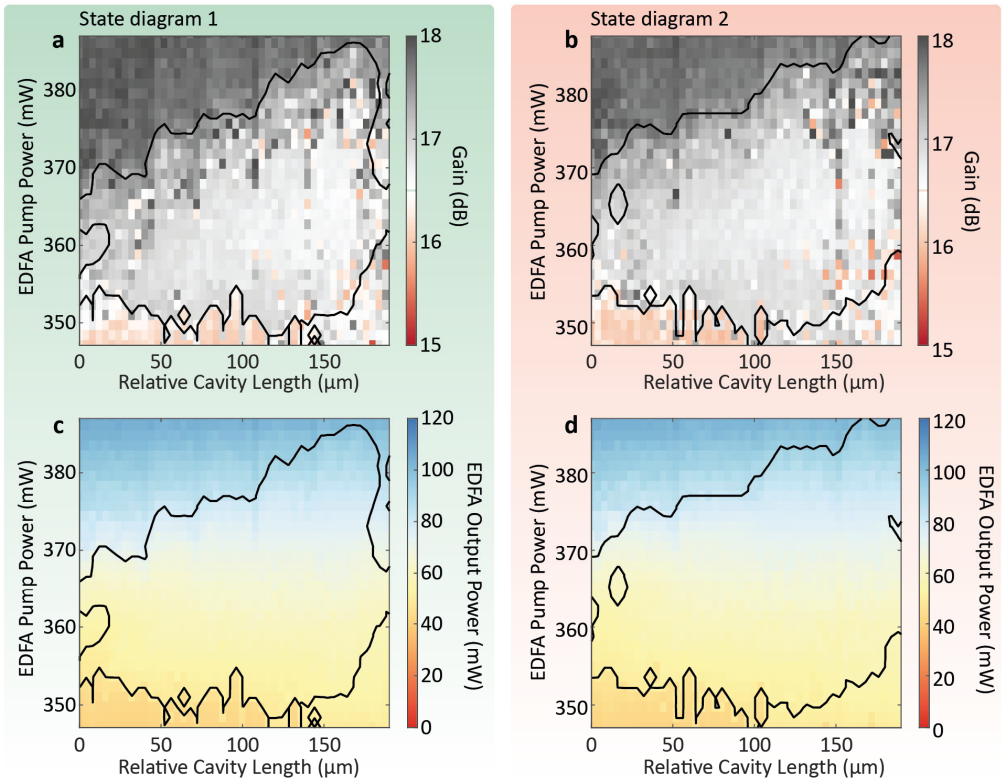

Figure E5 Additional measurements for the 'State Diagram 1 and 2' presented in Fig. S4a and c, respectively. **a** Optical gain of the EDFA for the 'State Diagram 1'. **b** Same as panel b, for the 'State Diagram 2'. **c** Intracavity power measured at the output of the amplifier or, equivalently, at the input of the microcavity, for the 'State Diagram 1'. **d** Same as panel c, for the 'State Diagram 2'.

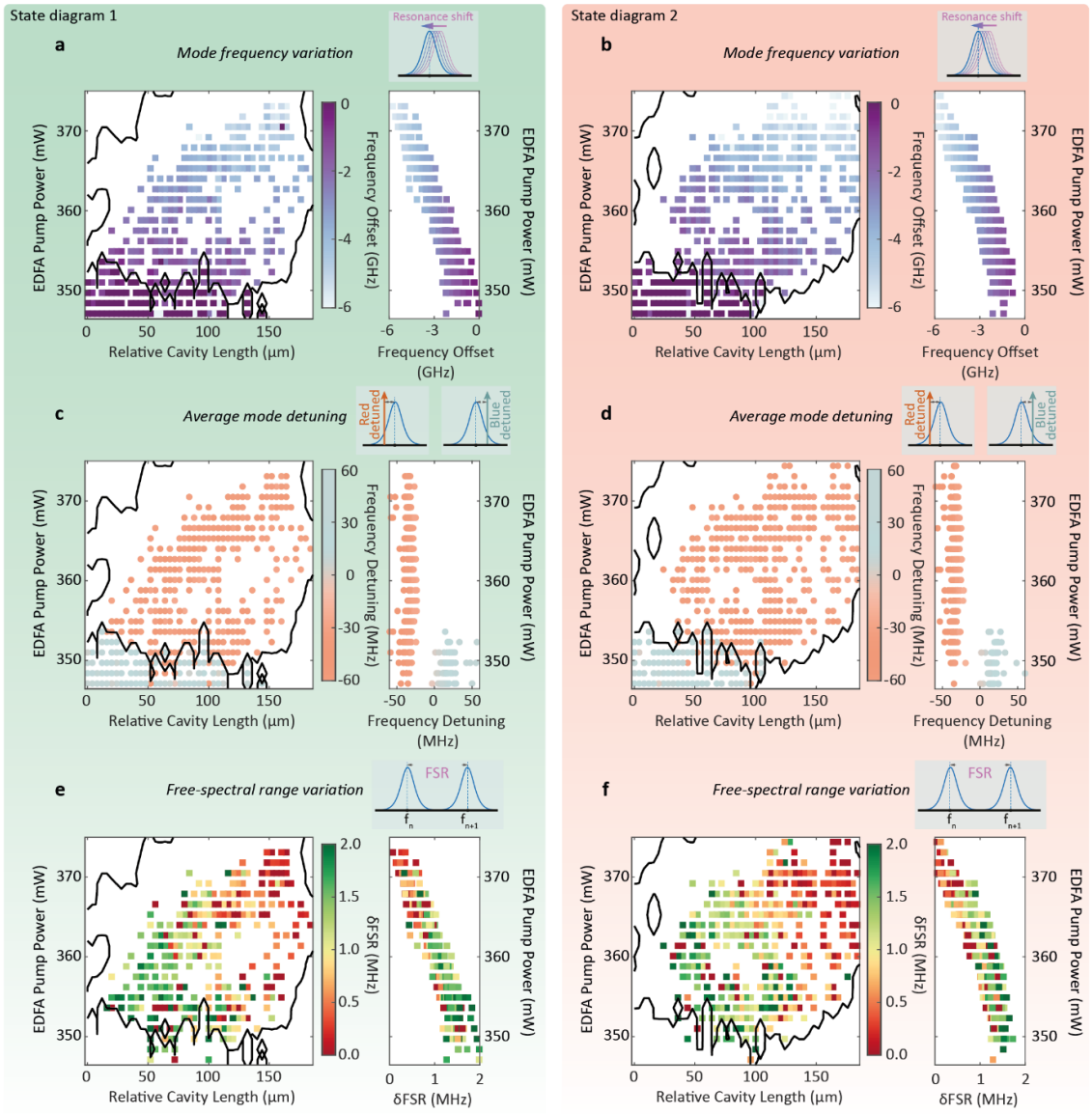

Figure E6 Analysis of the frequency positions of the stable states. Datas extracted from the laser scanning spectroscopy. Black lines mark soliton and CW region boundaries. **a** Variation of the frequency position of a selected resonance of the microcavity (here, we choose the mode centred approximately at 1543 nm). The colour code in the map follows the inset (right) showing the values of the frequency shift for the microcavity resonance. **b** Same as a, now for the 'State Diagram 2'. **c** Variation of the average detunings, calculated as the mean frequency difference between each oscillating microcomb laser line and the corresponding microcavity resonance centre across all microcomb lines. The colour code in the map follows the colours of the inset (right), where the values of the detunings versus EDFA pump power are shown. **d** Same as panel c, but for the 'State Diagram 2'. **e** Free-spectral range (FSR) variation associated with the soliton states (FSR~48.9 GHz) obtained across the mapped values. The colour code in the map follows the inset (right) showing the free-spectral range variation values. **f** Same as panel e, but for the 'State Diagram 2'.

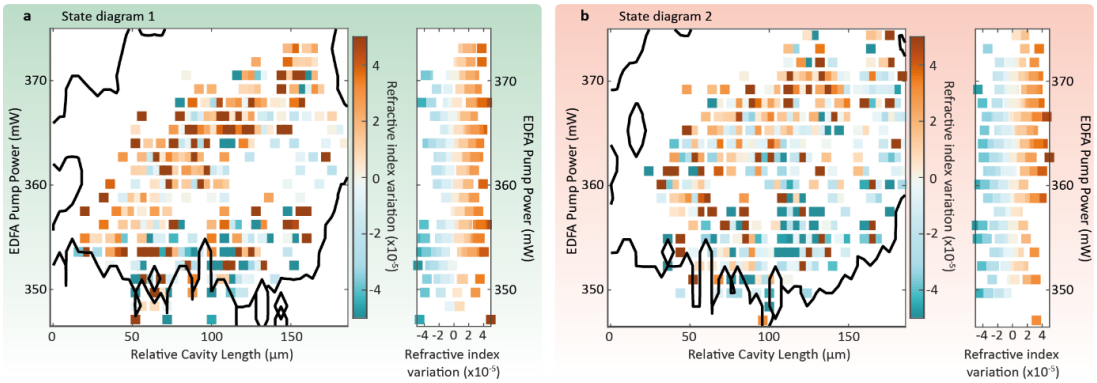

Figure E7 Analysis of the relative refractive index variation in the amplifier cavity. Here we show the relative refractive index variation of the amplifier under operating condition calculated as $\delta n_b n_b^{-1} = -\delta F\, F^{-1} - \delta L_b L_b^{-1}$. **a** Relative change of the refractive index for the soliton states obtained across the mapped values, extracted from the free-spectral range variation of the 'State Diagram 1'. The colour code in the map follows the inset showing the refractive index change. **b** Same as a for the 'State Diagram 2'.

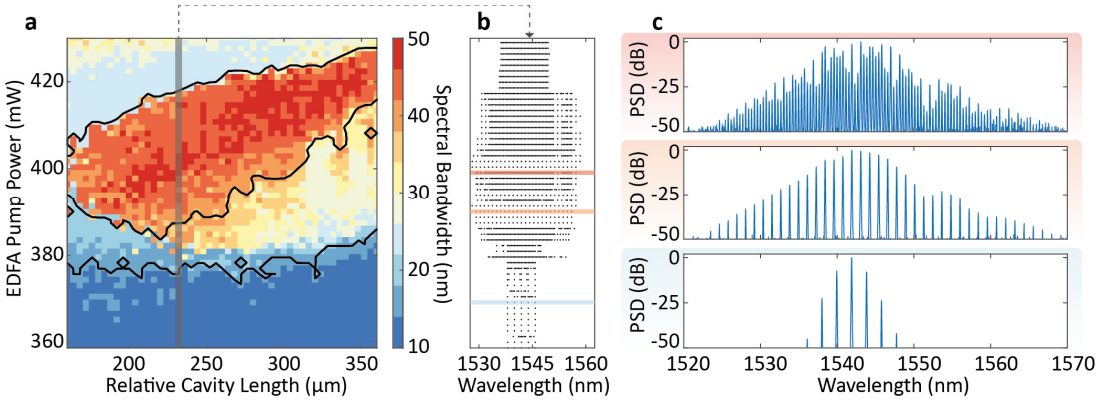

Figure E8 Experimental state diagram for a microresonator-filtered fibre laser with intracavity losses set to 14 dB. The delay axis uses the same zero definition as Fig. S4. **a** Spectral bandwidth (calculated as the bandwidth at -40dB from the maximum), in colour code, of the laser state as a function of the cavity length delay and EDFA pump power. Soliton states are found in the red region with the broadest bandwidths, while Turing patterns appear at the lowest EDFA values (in blue). The lasing regime is unstable outside these regions, which are roughly defined by the black border lines. During the experimental acquisition, the temperature was maintained at 40 °C within a fluctuation of a few degrees. **b** Optical spectra of the states at the delay 240 μm, identified by the vertical grey line in a. The black dots represent the frequency position relative to the maximum value of each comb mode. **c** From top to bottom, power spectral densities (PSDs) of the optical spectra for EDFA powers of 398 mW, 391 mW and 373 mW, respectively, as indicated by the corresponding coloured highlights in panel b.

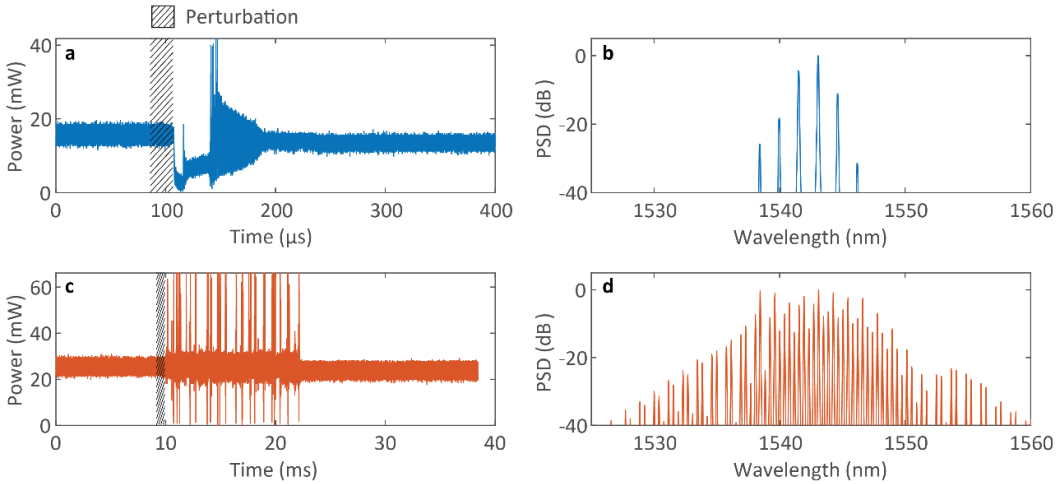

Figure E9 Perturbation recovery. The stationary state is perturbed with a steep variation in the voltage driving the EDFA pump power. **a** Recovery of a Turing pattern state. The power associated with the state is shown in blue, while the black shaded region indicates the time at which the EDFA pump power is modified to perturb the state. The system recovers to a state with similar average power and spectral shape after 0.1ms, which is in the temporal scale of the microcavity thermal nonlinearity response. **b** Corresponding optical spectrum of the recovered state in a. **c** Same as panel a, for a multi-soliton state. Note that the recovery time is on the order of 10 ms, dictated by the Erbium gain. **d** Corresponding optical spectrum for the recovered state in panel c.

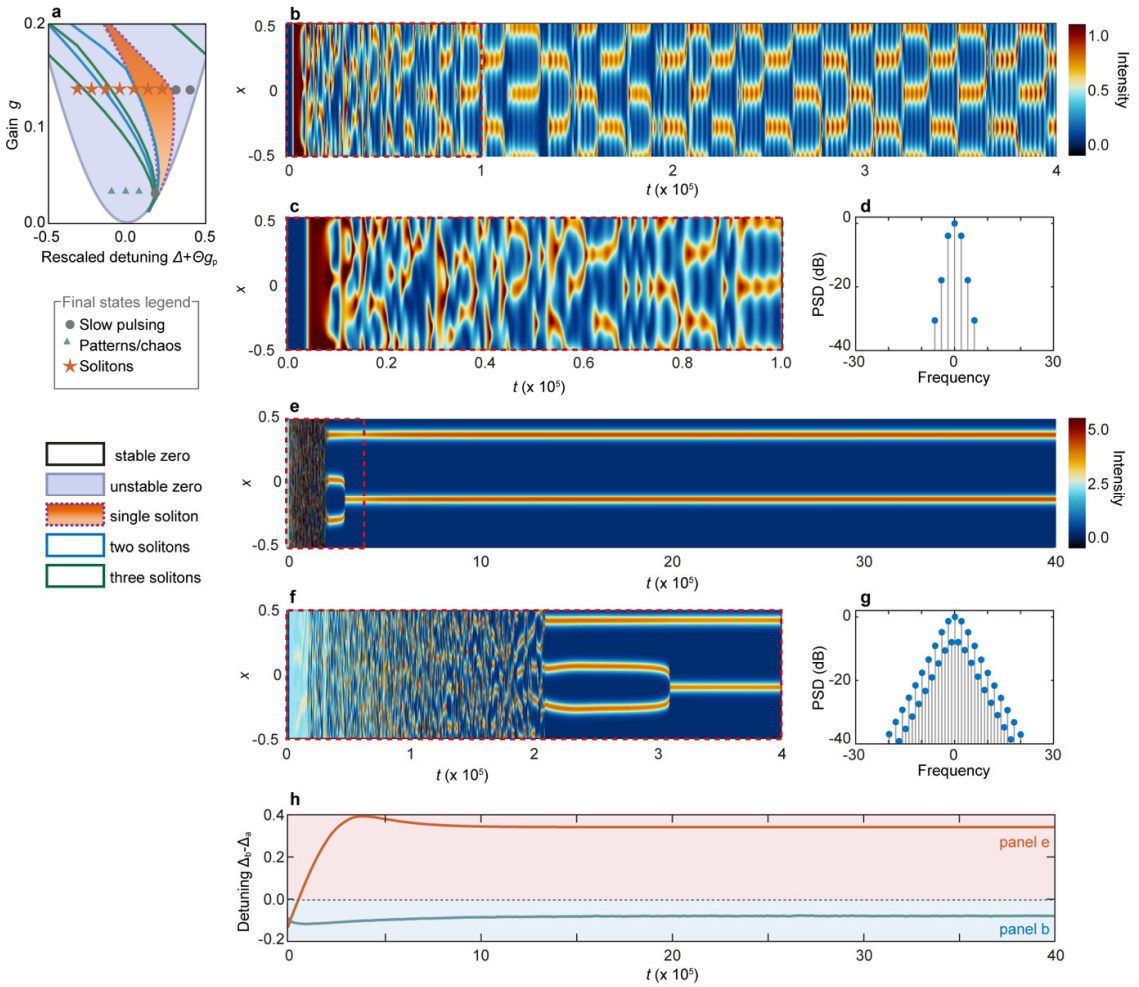

Figure E10 Start-up in the presence of gain-induced nonlinearity and thermal nonlinearity. a Stability region and a selection of steady states for the system. The colour of each marker represents the type of steady-state solution reached by the system after start-up from the noise for different values of the rescaled detuning $\Delta + \Theta g_P$ and gain g. **b** Pseudo-colour map of the electric field intensity in the microcavity as a function of the position in the microresonator x (normalised against the microcavity roundtrips) and time t (normalised against main-cavity roundtrips). The system parameters are $\Gamma_T = 2, \tau_T = 8 \times 10^3, \eta = 0.1, \tau_g = 4 \times 10^4, \Theta = -15, g = 0.03, \Delta + \Theta g_p = -0.0909$. **c** Enlarged view of panel b for the first 10^4 main-cavity roundtrips, highlighting the start-up of the pattern-like solution within a timescale compatible with the thermal time constant $\tau_T = 8 \times 10^3$. **d** Output power spectral density (PSD) of the a field. **e-g** Same as panels b,c and d, but for parameters $\Gamma_T = 2, \tau_T = 8 \times 10^3, \eta = 0.1, \tau_g = 4 \times 10^4, \Theta = -15, g = 0.135, \Delta + \Theta g_p = -0.1342$. Panel f illustrates the start-up of the two-soliton state from noise within a time-frame compatible with the slower timescale $\tau_g = 4 \times 10^4$. **h** Temporal evolution of the effective detuning $\Delta_b - \Delta_a$ for the low-gain pattern-like states (blue line) and the two-soliton states (orange line).